Tellus
SERIES A
DYNAMIC
METEOROLOGY
AND OCEANOGRAPHY
PUBLISHED BY THE INTERNATIONAL METEOROLOGICAL INSTITUTE IN STOCKHOLM

Tellus (2009), 61A, 512–526

TELLUS

Fine structure of a Greenland reverse tip jet: a numerical simulation

By TADAYASU OHIGASHI* and G. W. KENT MOORE, *Department of Physics, University of Toronto, Toronto, ON, Canada*

(Manuscript received 17 December 2007; in final form 2 March 2009)

ABSTRACT

Reverse tip jets are strong low-level winds with easterly component that form near the southern tip of Greenland. In the present study, a reverse tip jet case which occurred from 21 to 22 December 2000 was examined to clarify its fine structure using a numerical model with a horizontal resolution of 3 km. The reverse tip jet, showing the supergeostrophic wind speed with a maximum wind speed in excess of 45 m s^{-1}, extended from the east coast of Greenland to the west of Cape Farewell with anticyclonic curvature. A cloud free region coincided with the jet indicated that there was a mesoscale downdraft. Along the eastern edge of the jet, a banded cloud formed between the upstream easterly wind and the colder northerly wind that is a part of the jet and is located along the east coast. This cloud was associated with large gradients in surface wind speed, temperature, moisture, and heat flux. A maximum surface total heat flux of 300 W m^{-2} coincided with the location of the jet. It is suggested that the orographic deflection by Greenland's large-scale topography as well as small-scale downslope winds behind mountains with fiords causes the reverse tip jet.

1. Introduction

Topography is an important factor that influences atmospheric dynamics. One class of weather systems associated with topography are strong low-level winds. High wind speeds at the ocean's surface can cause large heat, moisture, and momentum exchanges between the ocean and atmosphere, which can impact circulations in both fluids. The stationary nature of the topographic forcing can lead to high winds in a local region that can over time amplify these fluxes leading to climatologically important effects.

Strong winds associated with topography are classified into downslope winds (e.g. Lilly, 1978; Saito and Ikawa, 1991), barrier winds (e.g. Parish, 1982; van den Broeke and Gallee, 1990; O'Connor et al., 1994; Moore and Renfrew, 2005), gap winds (e.g. Saito, 1993; Jackson and Steyn, 1994a,b; Steenburgh et al., 1998; Pan and Smith, 1999; Flamant et al., 2002; Sharp and Mass, 2002; Gaberšek and Duran, 2004, 2006), tip jets (Doyle and Shapiro, 1999; Moore, 2003; Pickart et al., 2003; Moore and Renfrew, 2005), and reverse tip jets (Moore, 2003; Moore and Renfrew, 2005; Martin and Moore, 2007). Downslope and barrier winds are strong winds blowing down the slope and parallel to the barrier on the windward side of a mountain range, respectively. Gap winds are a strong low-level jet blowing in a channel between mountains or a gap in a mountain.

Reverse tip jets are among the most recently identified of these weather systems. They have been observed to form in the vicinity of Cape Farewell, which is located at the southern tip of Greenland (Fig. 1a). This area is of climatological importance because of the observations that deep ocean convection associated with the return branch of the thermohaline circulation occurs both to the east (Pickart et al., 2003) and west (Lavender et al., 2002) of Cape Farewell. A related phenomenon that forms in the same region are tip jets which are strong low-level winds with westerly component. Doyle and Shapiro (1999) pointed out the existence of tip jets from numerical simulations. Moore (2003) used the National Centers for Environmental Prediction (NCEP) reanalysis data to show that low-level strong winds with easterly component also form in the area. This flow with easterly component was given the name of reverse tip jet to distinguish it from the tip jets identified by Doyle and Shapiro. Moore and Renfrew (2005) examined a climatology of 10 m winds, derived from the Quik-SCAT scatterometer data, around the southern tip of Greenland. From this data, they confirmed Moore's analysis that there are two predominant wind directions corresponding to tip jets and reverse tip jets.

Moore (2003) also used composite sea-level pressure distributions for tip jets and reverse tip jets to show that both form as the result of the interaction of a synoptic-scale cyclone with the high topography of southern Greenland. In the case of tip jets, the cyclone centre was typically located to the northeast

*Corresponding author.
e-mail: ohigashi@rain.hyarc.nagoya-u.ac.jp
DOI: 10.1111/j.1600-0870.2009.00399.x

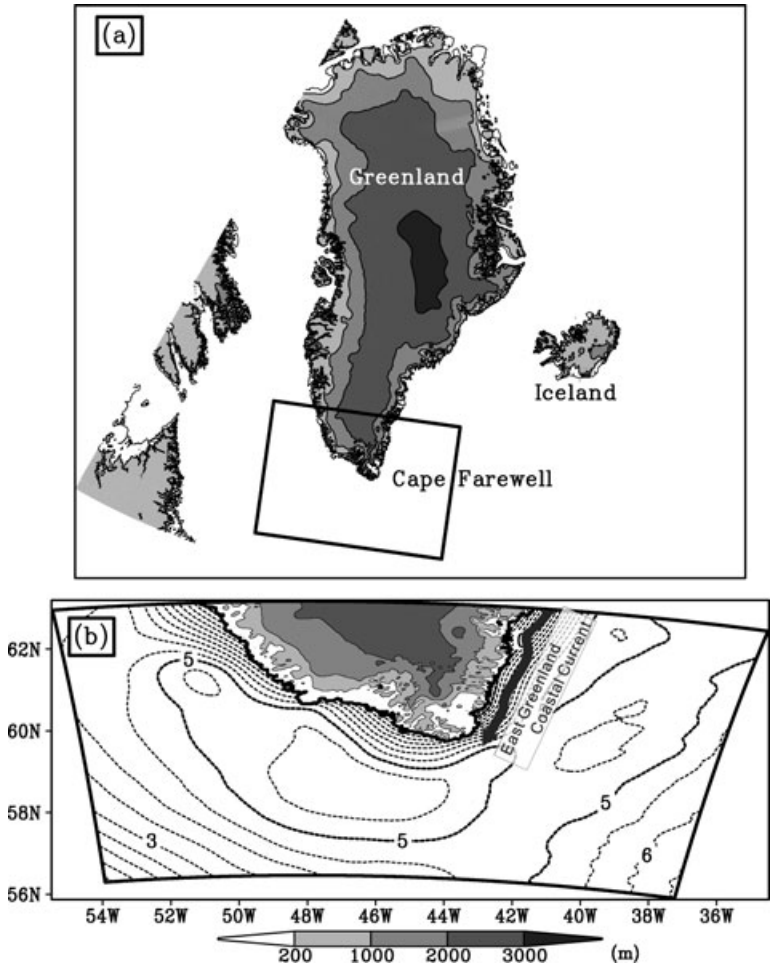

Fig. 1. (a) Topography of whole Greenland (m). A rectangle shows the simulation domain. (b) Topography in the simulation domain (solid lines and grey levels, m) and sea surface temperature (dashed lines, °C) simulated using CReSS at 0000 UTC, 22 December 2000. The dashed contour interval is 0.5 °C and the thick contour line is drawn every 5 °C. A solid arrow indicates the East Greenland Coastal Current.

of Cape Farewell. On the other hand for reverse tip jets, the cyclone centre was present to the south of Cape Farewell. This difference in the location reflects the impact that rotation plays in the generation of both classes of jets. Tip jets and reverse tip jets show the highest probability of occurrence, about 10%, during the winter. This corresponds to the season during which extra-tropical cyclones between southern Greenland and Iceland (within the climatological Icelandic low) show a maximum count and develop deeper than those in summer (Serreze et al., 1997). During summer, the probabilities of occurrences of both classes are almost zero. In addition, there is interannual variability in the formation frequency of tip jets and reverse tip jets. This variability is related to the phase of the North Atlantic Oscillation (NAO). In the positive NAO mode, tip jets are common and reverse tip jets are less common. The opposite tendencies occur in the negative NAO phase (Pickart et al., 2003; Moore, 2003).

Regarding the formation mechanism for reverse tip jets, Moore and Renfrew (2005) suggested that barrier winds, which are caused by an orographic deflection of flows with sufficiently large non-dimensional mountain height, is a possible mechanism. The non-dimensional mountain height $\hat{h}$ is a dimensionless number defined as Nh/U, where N is the Brunt–Väisälä frequency in the upstream region, h is the height of the mountain and U is a wind speed component across an mountain (e.g. Baines, 1987; Chen and Smith, 1987; Saito, 1993). The non-dimensional mountain height $\hat{h}$ more than 1 indicate that some of an upstream flow is blocked by an mountain.

They also showed anticyclonic turning of wind directions along the streamline is a feature of reverse tip jets. They explained that, assuming the gradient wind balance and anticyclonic flow within reverse tip jets, the flow is supergeostrophic, that is a greater wind speed than the geostrophic wind speed, and the surpergeostrophic flow corresponds to the core of reverse tip jets, although this balance condition does not explain the acceleration processes. For tip jets, Doyle and Shapiro (1999) proposed that the acceleration of the horizontal wind speed that lead to the jet was associated with the conservation of the Bernoulli function in the descending motion behind the topographic barrier. They also showed the importance of an orographic deflection. Moore and Renfrew (2005) mentioned that composites of surface winds have a possibility to include cases composed of both mechanisms.

For reverse tip jets, much of the research has been focused on describing their climatological features (Moore, 2003; Moore and Renfrew, 2005). These climatologies do not necessarily reflect a single case, and the features might be a superimposition of two or more characteristic fields. In addition, the horizontal resolution of the data used in the studies are possibly too coarse to capture the fine scale structure of these jets and also provide no information on their vertical structure. Martin and Moore (2007) is the only case study of a reverse tip jet at present. They used a numerical model with horizontal resolutions of 18 and 6 km and focused on air-sea interaction associated with a reverse tip jet. In the present study, we will pay attention to fine horizontal and vertical structures of a reverse tip jet case. A numerical model with a horizontal resolution of 3 km is used to clarify the fine scale features.

2. Model

The Cloud Resolving Storm Simulator (CReSS) developed at Hydrospheric Atmospheric Research Center of Nagoya University was used (Tsuboki and Sakakibara, 2002, 2007). The CReSS model has been used to simulate many atmospheric phenomena (e.g. Liu et al., 2004; Wang et al., 2005; Liu et al., 2006; Maesaka et al., 2006; Zhang et al., 2006; Ohigashi and Tsuboki, 2007; Yamada et al., 2007a,b; Endo et al., 2008; Yamada, 2008). CReSS is a limited-area model formulated with compressible and non-hydrostatic equations with a terrain following vertical coordinate. The domain was projected on a plane using polar stereographic projection and a map factor was used for spatial differential. No cumulus convection parametrization is used, rather cloud microphysical processes are explicitly represented with a bulk method of cold rain parametrization to predict mixing ratios of cloud water, rain, cloud ice, snow, and graupel and number densities of cloud ice, snow, and graupel. A subgrid scale diffusion is computed using the 1.5 order closure model, in which the turbulent kinetic energy is calculated using a prognostic equation. Categories of land use are land covered by snow and sea. Sea ice was not included because no significant sea ice was identified in the vicinity of the area in which the reverse tip jet was seen. Ground and sea temperatures are calculated using the one-dimensional heat diffusion equation. A grid of $352 \times 250 \times 42$ was used in the simulation. The horizontal grid space is 3 km at 60°N. The vertical grid spacing varied from 100 m at the surface to 420 m at the top of the model at 12 391 m. The upper boundary was a rigid wall condition. There is a sponge layer above a height of 6300 m. For the lateral boundary, the radiative condition was adopted and a relaxation zone was set up with a width of 120 km at the edge of the model domain.

With regard to the initial and boundary data for the CReSS simulation, a simulation result of the Fifth-Generation NCAR/Penn State Mesoscale Model (MM5) (Grell et al., 1995) was utilized. In the MM5 simulation, two domains with horizontal grid spaces of 18 km (Domain 1) and 6 km (Domain 2) were assigned. Domain 1 was one-way nested in the regional analysis of Canadian Meteorological Center (CMC), and Domains 1 and 2 were calculated with a two-way interface. Boundary conditions including sea surface temperature (SST) data were also provided by the CMC's data. Sea ice was also not considered in this simulation. A cumulus convection parametrization scheme was applied for Domain 1 while no cumulus parameterization was used for Domain 2. A bulk cold rain parametrization was applied for both the domains. The MM5 simulation was initialized at 0000 UTC, 21 December 2000. The other detailed configuration of the MM5 simulation is the same as that described in Martin and Moore (2007). They compared the wind fields at a 10 m height of their results with the Quik-SCAT 10 m wind fields, and states their simulation is overall agreement with the Quik-SCAT wind fields except that the simulated wind speed is 5–10 m s^{-1} smaller than the Quik-SCAT retrieved wind speed. In this regard, Moore et al. (2008) have shown through a comparison with meteorological buoy data from the Cape Farewell region that the Quik-SCAT retrieved wind is biased high in high wind speed conditions such as occur during tip jets and reverse tip jets.

The simulation results every 1 h with Domain 2 were used for the CReSS simulation. The CReSS simulation was integrated for 12 h from 12 UTC, 21 December 2000. In this integration, the mode-splitting scheme (Klemp and Wilhelmson, 1978) with small and large time steps was adopted. The small time step integration used for the acoustic wave modes is solved explicitly in horizontal and implicitly in vertical. With respect to the large time step, the leap-flog scheme with the Asselin time filter (Asselin, 1972) is adopted. The small and large time steps were 2 and 6 s, respectively.

3. Comparison with observations

Figure 2a is the Quik-SCAT 10 m wind fields at 2137 UTC, 21 December 2000, which is a product of the National Aeronautics and Space Administration (NASA). The simulated 10 m wind fields at 2140 UTC, 21, which corresponds to the time of the Quik-SCAT data, are also shown in Fig. 2b. The strong wind speed along the east coast and its extension to the west, which indicate a reverse tip jet, are shown with the wind over 18 m s^{-1} in both of observation and simulation. In the west of Greenland, a wake with wind speed less than 12 m s^{-1} is present and successfully expressed in the simulation. The maximum wind speed in the simulation is smaller than the Quik-SCAT retrieved wind, which is the same as the parent model results (Martin and Moore, 2007) and is consistent with the results of Moore et al. (2008). The strong wind region over 24 m s^{-1} in the southwest of Cape Farewell extends to the north in the simulation while it is relatively narrow in the Quik-SCAT. The deflected northerly wind direction along the east coast is not so remarkable in the Quik-SCAT wind field, which may be the result of

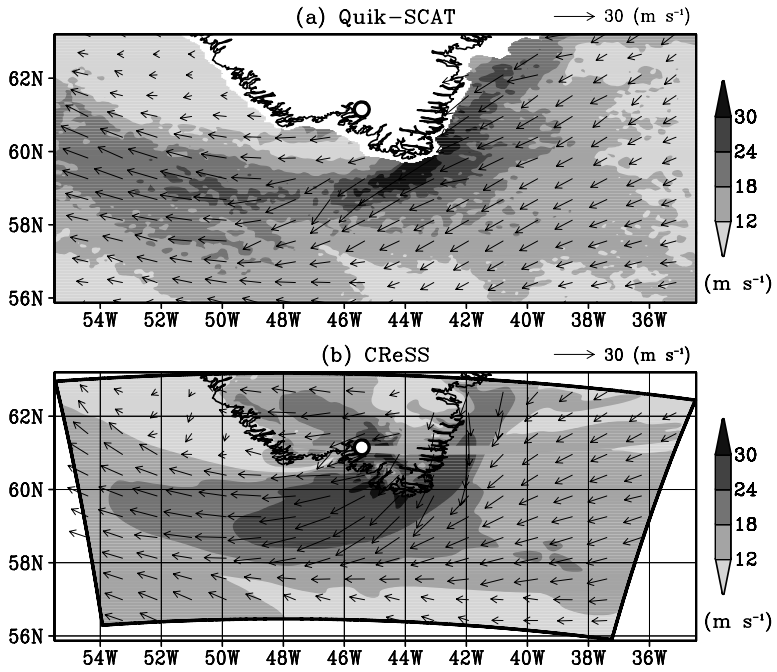

Fig. 2. (a) Quik-SCAT 10 m wind field (arrows and grey levels, m s^{-1}) at 2137 UTC, 21 December 2000. (b) Simulated 10 m wind field (arrows and grey levels, m s^{-1}) at 2140 UTC, 21 December 2000. Open circles indicate the sounding observation site of Narsarsuaq.

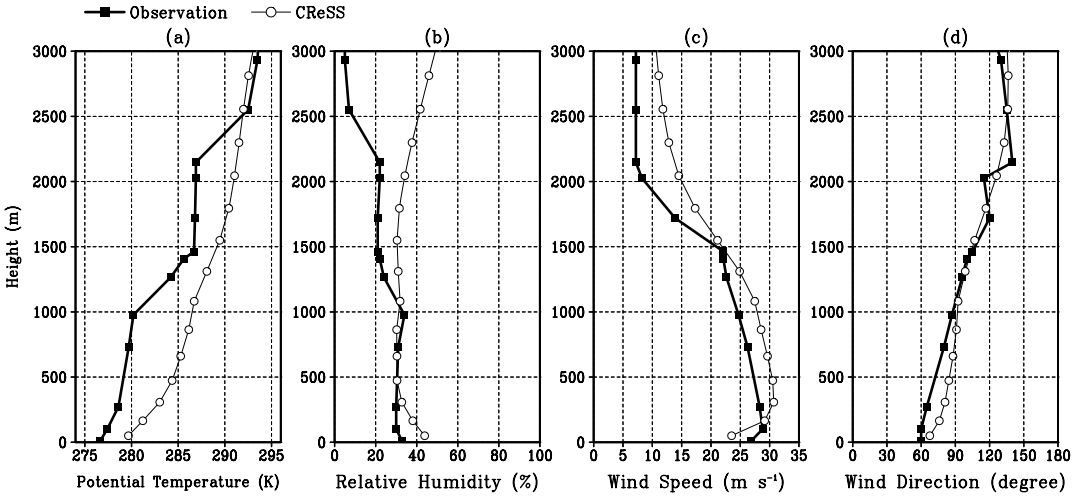

Fig. 3. Vertical profiles of (a) potential temperature (K), (b) relative humidity (%), (c) wind speed (m s^{-1}) and (d) wind direction (degree) at 00 UTC, 22 December 2000. Thick lines with solid rectangles are obtained from sounding observation at Narsarsuaq (61.15°N, 45.43°W; open circle shown in Fig. 2a), and thin lines with open circles show simulated fields averaged within 1° in the meridional direction and 0.5° in the zonal direction centred at 61.15°N and 45.43°W (open circle shown in Fig. 2b).

difficulty in retrieving wind speed and direction data close to the coast.

The low-level sounding profile at 00 UTC, 22 December 2000 at Narsarsuaq (61.15°N, 45.43°W) is shown in Fig. 3. Narsarsuaq is located in the leeward (southwest) side of the island and marked with open circles in Fig. 2a. The simulated field is averaged within 1 degree in the zonal direction and 0.5° in the meridional direction centred at the location of Narsarsuaq (Fig. 2b). For the potential temperature profile (Fig. 3a), the simulation fields (thin line with open circles) are 3–7 K higher than the observation (thick line with solid rectangle) below a height of 2500 m. The Brunt-Väisälä frequency, that is an indicator of a stability of atmosphere, between the surface to a height of 2500 m is 0.0135 s^{-1} in the model and 0.0148 s^{-1} in the observations. This appears not to be a significant difference. The difference between the simulation and observation in relative humidity (Fig. 3b) is less than 15% below a height of 2200 m, and both show a dry condition (about 20–40%). The wind speed (Fig. 3c) of the simulation is a few to 7 m s^{-1} higher than the observation except for that in the lowest level. However, both the patterns

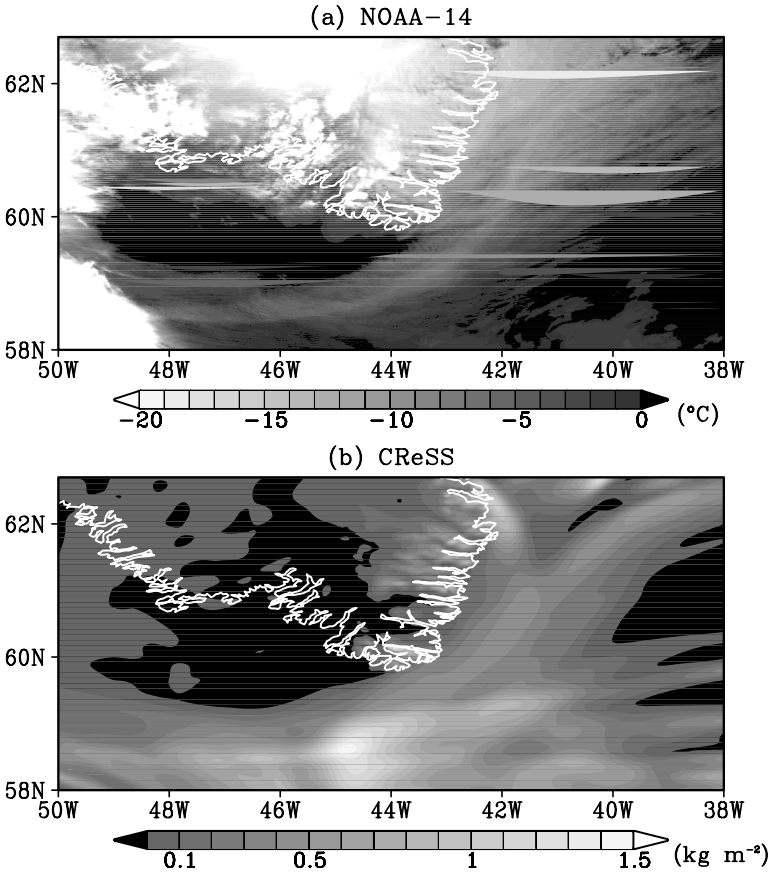

Fig. 4. (a) NOAA-14 Channel 4 satellite image at 1819 UTC, 21 December 2000. (b) Vertically integrated hydrometeor field (kg m^{-2}) at 1820 UTC, 21 December 2000 obtained from the numerical simulation.

show the maximum wind below a height of 500 m with about 30 m s^{-1} and gradually decrease with height. The wind direction (Fig. 3d) in both fields changes clockwise from ENE near the surface to SE around a height of 2500 m. Although there are some differences in the absolute value between the simulation and observation, the patterns in the low level in the simulation represent the characteristics of observation.

The cloud pattern associated with the reverse tip jet is shown in Fig. 4. NOAA-14 channel 4 image (Fig. 4a) as well as vertically integrated hydrometeors (Fig. 4b), which is the vertical integration of the total mixing ratio of cloud water, rain, cloud ice, snow and graupel, provide the information on the horizontal distribution of clouds (Maesaka et al., 2006). One of the characteristic clouds is broad cloud band seen along about 100 km off the east coast and extending to the west in the south of the island (Fig. 4a), which is also identified in the simulation (Fig. 4b). To the north of this cloud band, there is a cloud free region extending to the west of Cape Farewell. This is also identified in both the satellite image and simulated fields.

4. Reverse tip jet structure

The topography in southern Greenland within the simulation domain is shown in Fig. 1b. High topography is present inland. There are many fiords with deep valleys within approximately 100 km of the coastline. Figure 1 also shows the sea surface temperature (SST) field simulated using CReSS at 0000 UTC, 22 December 2000. We focus our analysis on this time, in which the wind speed in the reverse tip jet was a maximum. The SST was between 2 and 6.5 °C within the domain except near the coast where it was lower as a result of the cold waters of the East Greenland Coastal Current. A local maximum in the SST field is present a few hundred kilometers southwest of Cape Farewell. A maximum difference between the SST at this time and the initial time is less than 1 °C implying that changes in the SST field over the period of the simulation are not large.

When the synoptic-scale cyclone moved from Labrador toward Iceland, the isobars in the lower troposphere extended in the WNW–ESE direction with a high pressure region in the north (Fig. 5). This resulted in easterly flow in the region of interest. The pressure gradient is large on the windward side (eastern side) of Greenland, while it is small on the leeward side (western side). This pattern is most striking near the surface (Fig. 5c). The asymmetric pressure gradient is not so clear at a height of 2555 m (Fig. 5a) and is confined below the inland topography of Greenland. In addition, the wind fields to the east of Greenland show a large northerly component near Greenland especially in the lower levels. Therefore, the wind vectors are directed toward

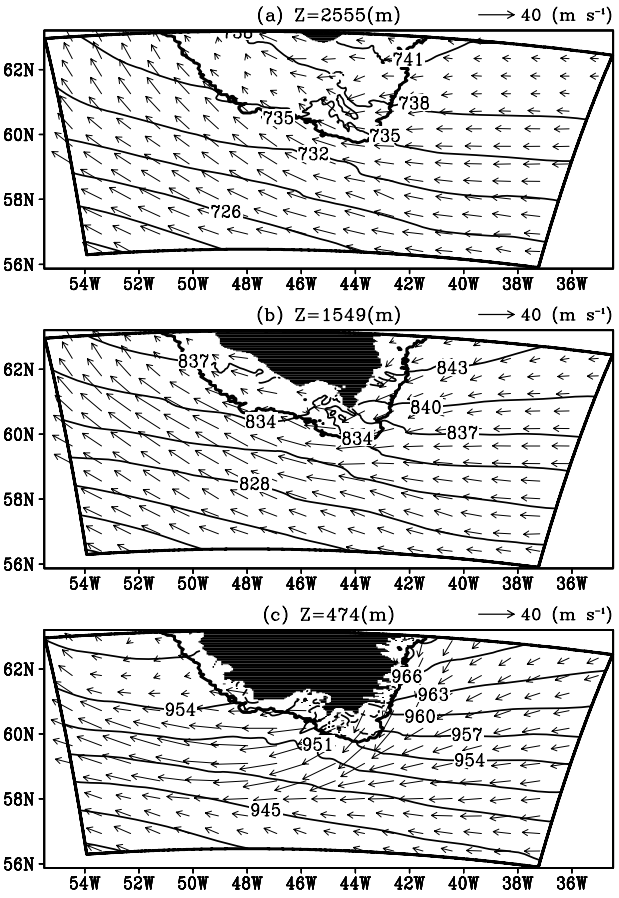

Fig. 5. Pressure (solid lines, hPa) and horizontal velocity vectors (arrows) at heights of (a) 2555 m, (b) 1549 m and (c) 474 m at 0000 UTC, 22 December 2000 obtained from the numerical experiment. The contour interval is 3 hPa. Areas below ground at each height are shaded black.

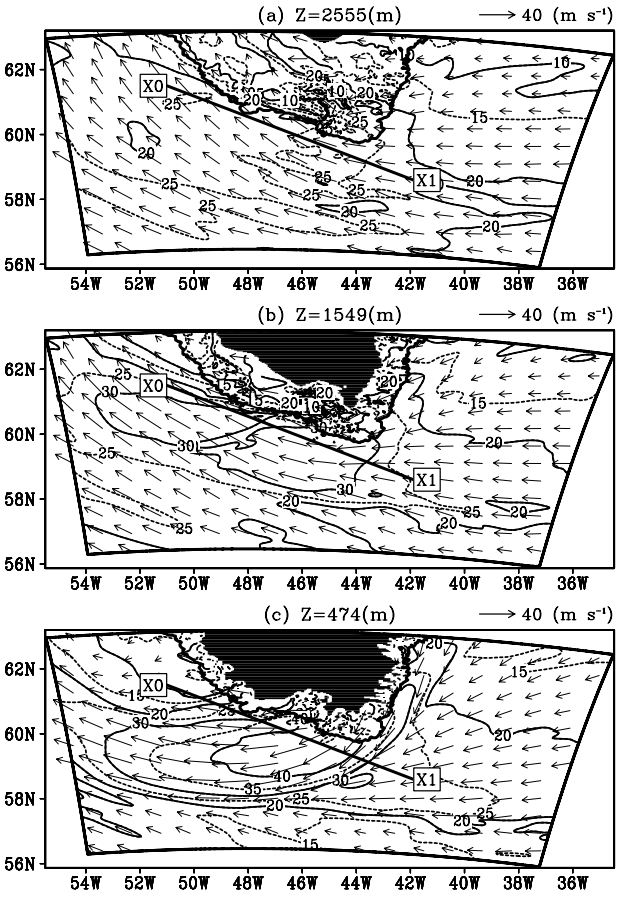

Fig. 6. Horizontal velocity vectors (arrows) and wind speed (contours, m s^{-1}) at heights of (a) 2555 m, (b) 1549 m and (c) 474 m at 0000 UTC, 22 December 2000 obtained from the numerical experiment. The contour interval is 5 m s^{-1}. Areas below ground at each height are shaded black.

the low pressure side. To the west of Cape Farewell, the wind vectors turn anticyclonically along the streamline of the jet, and are finally directed toward high pressure side. This anticyclonic turning of wind direction is in agreement with the wind fields shown in Moore and Renfrew (2005), although they showed a composite pattern of reverse tip jets at the surface.

The maximum wind speed at a height of 2555 m is more than 20 m s^{-1} in a large area to the south of Cape Farewell (Fig. 6a). At a height of 1549 m (Fig. 6b), there exists a wind speed maximum in excess of 30 m s^{-1} that extends along the southwest coast of Greenland to the west of Cape Farewell. In the lowest level (Fig. 6c), the strong wind field extends westward from the southern edge of Greenland along the anticyclonically turning flow. The wind speed is over 40 m s^{-1} within about 300 km of the southwest coast of Greenland with the largest wind speeds in excess of 45 m s^{-1}. These strong winds with easterly component are referred to as the 'reverse tip jet' in the present study. The reverse tip jet forms from the east coast of Greenland, where the wind direction was with relatively large northerly component, toward the southwest of Cape Farewell. A region of low wind speed in the lee of Greenland near 62°N is also apparent, especially at the lowest level. Wind speeds in this wake are less than 10 m s^{-1}. The wind speed and geostrophic wind speed were almost equal at 62°N, 38°W that is located in the upstream. The wind speed was 15 m s^{-1}.

The vertical cross section of wind speed along the line X0-X1 in Fig. 6 is shown in Fig. 7. In the vicinity of the reverse tip jet (centred at a distance from X0 of approximately 350 km), the wind speed gradually increases downward below a height of 3500 or 4000 m reaching a maximum in excess of 40 m s^{-1} at a height of approximately 500 m. Below this height, the wind speed decreases because of the presence of the surface. As one can therefore see, the reverse tip jet is confined below a height of a few kilometres. This vertical extent corresponds to the inland height of the Greenland's topography. The wake to the northwest

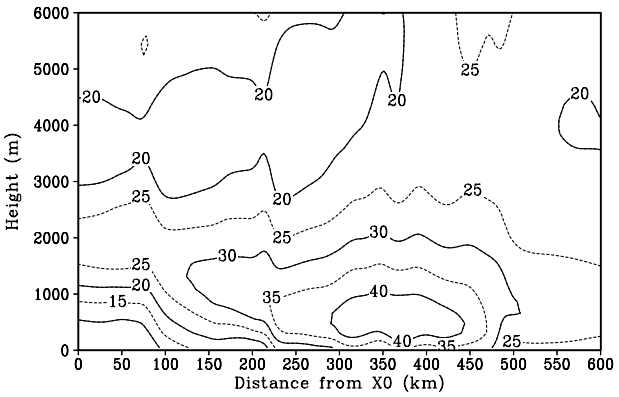

Fig. 7. Vertical cross section of horizontal wind speed along the line X0-X1 in Fig. 6 at 0000 UTC, 22 December 2000 obtained from the numerical experiment. The contour interval is 5 m s^{-1}.

of the reverse tip jet can be also seen at a distance from X0 less than 100 km.

Figure 8 shows the difference between wind speed and geostrophic wind speed at low levels. Upstream of Cape Farewell at 62°N, 38°W, the difference is almost zero, which indicates the flow is in geostrophic balance. Along the southeast coast of Greenland, the winds are for the most part subgeostrophic. On the other hand, supergeostrophic winds are present to the southwest of Cape Farewell. The location of this supergeostrophic flow is collocated with the core of the reverse tip jet. The wind speed in the core of the reverse tip jet is more than 25 m s^{-1} larger than the geostrophic wind speed, and indicates that the flow is highly supergeostrophic. Farther downstream along the streamline, the highly supergeostrophic wind speed is reduced and approaches the geostrophic wind speed. The relationship between the wind speed and geostrophic wind speed to the formation of the reverse tip jet will be discussed in Section 5.

The vertically integrated hydrometeor field corresponding to the cloud patterns is shown in Fig. 9. The most pronounced feature is the banded element present off the southeast coast of Greenland. This band is extending toward the southwest along the eastern edge of the reverse tip jet. The core of the reverse tip jet shows cloud free with again some clouds present along its northern limit. These cloud features were confirmed in the other simulation times (Fig. 4b) and the satellite image (Fig. 4a).

In order to clarify the vertical distribution of hydrometeors, the total mixing ratios of hydrometeors at three levels are shown in Fig. 10. Along the banded feature seen in Fig. 9, large total mixing ratio are present at all levels with the highest values occur at a height of 1549 m (Fig. 10b). On a height of 2555 m, the significant mixing ratio was also seen along the band while no significant mixing ratio was seen to the east of the band. This indicates that the band was relatively deep as compared with

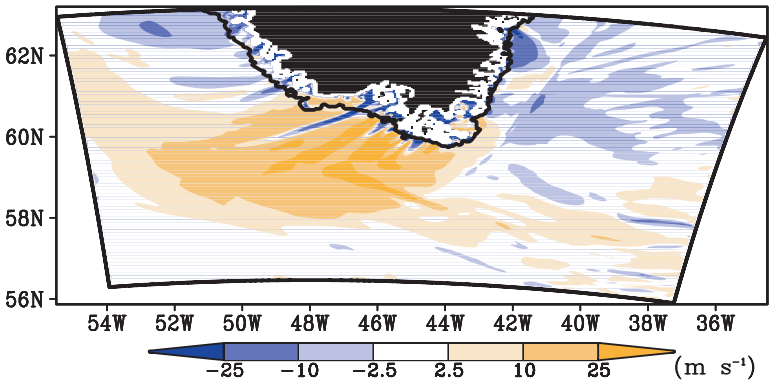

Fig. 8. Difference between wind speed and geostrophic wind speed (m s^{-1}) at a height of 474 m at 0000 UTC, 22 December 2000 in the numerical experiment. Areas below ground at each height are shaded black.

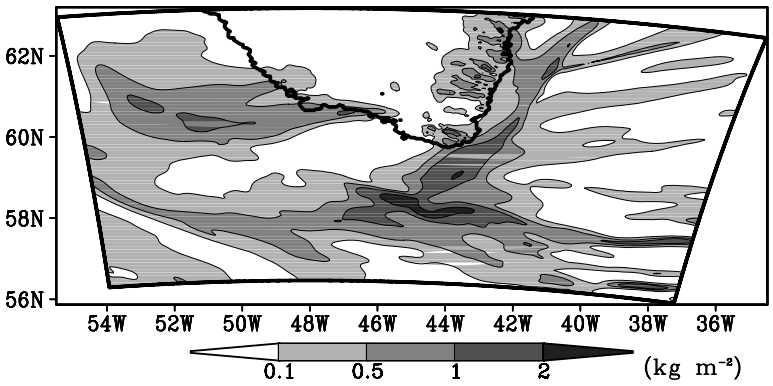

Fig. 9. Vertically integrated hydrometeor field (kg m^{-2}) at 0000 UTC, 22 December 2000 in the simulation experiment.

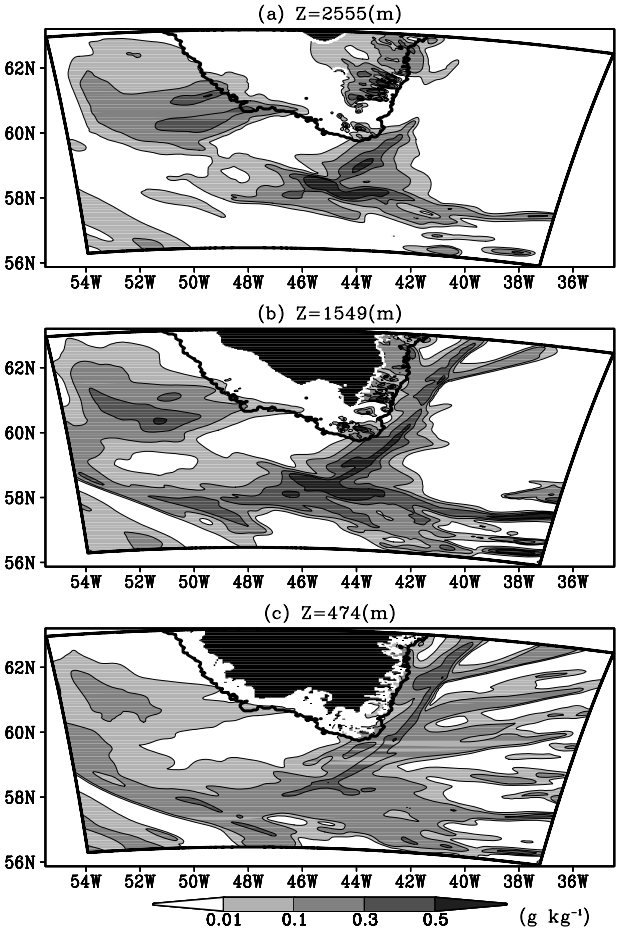

Fig. 10. Total mixing ratio of hydrometeors (g kg^{-1}) at heights of (a) 2555 m, (b) 1549 m and (c) 474 m at 0000 UTC, 22 December 2000 in the numerical experiment. Areas below ground at each height are shaded black.

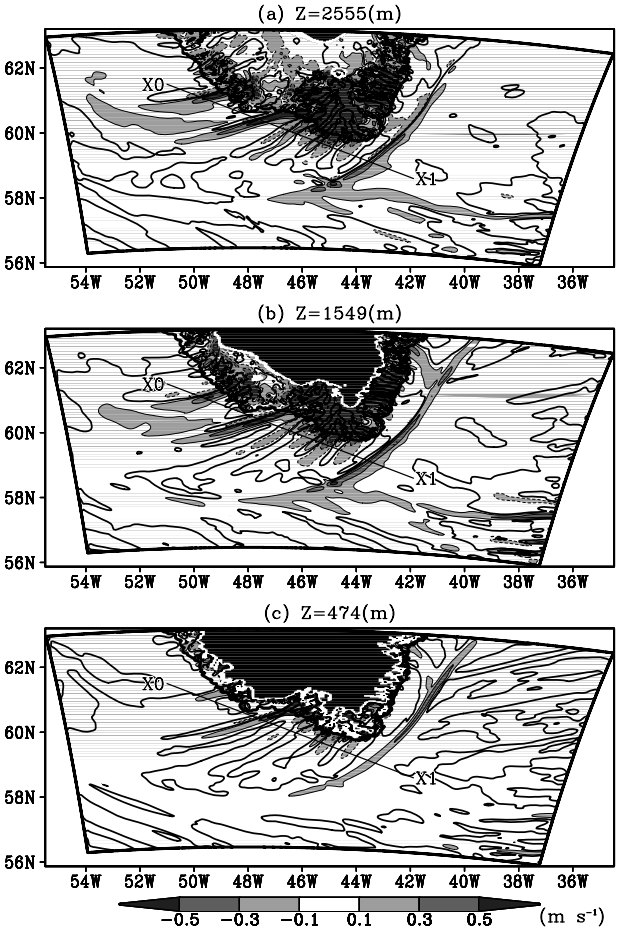

Fig. 11. Vertical velocity (m s^{-1}) at heights of (a) 2555 m, (b) 1549 m and (c) 474 m at 0000 UTC, 22 December 2000 obtained from the numerical experiment. Thin solid, thick solid, and broken contours indicate positive, zero, and negative values, respectively. Areas below ground at each height are shaded black.

the upstream cloud region extending to the east of the band. To the north of the reverse tip jet region with the cloud free, hydrometeors are again present at all levels with the largest values occurring at 1549 m. At 2555 m, two pronounced plumes of high hydrometeor mixing ratio extend westward from the southwest coast of Greenland.

These hydrometeors are strongly correlated with features in the vertical velocity field (Fig. 11). In the region corresponding to the reverse tip jet which coincides with the cloud free region, predominant descending motion extends most offshore in the low level (Fig. 11c). A robust updraft of more than 0.1 m s^{-1} is formed along the east coast of Greenland and eastern edge of the reverse tip jet with the maximum velocity of 0.5 m s^{-1}, and the width of the updraft more than 0.1 m s^{-1} is a few tens kilometres. This updraft corresponds to the band of large mixing ratio of hydrometeors shown in Figs. 9 and 10. To the east of this updraft, there are weak shallow updrafts corresponding to shallow clouds. Another remarkable feature is the alternating upward and downward motions which show the maximum amplitudes near the coastline and extend offshore from the southwest coast of Greenland. The wave-like updrafts form the plumes of hydrometeors to the north of the reverse tip jet, while there is no hydrometeor within the mesoscale descending motion coinciding with the reverse tip jet (Figs. 9 and 10).

The vertical cross section of this wave-like vertical wind along the line X0–X1 in Fig. 11 shows that the ascending and descending motions extend to a height of 5 km from the surface (Fig. 12a). Updrafts and downdrafts alternately appear in the vertical direction in a manner that is similar to what is found in a gravity wave generated by an obstacle (e.g. Cotton and Anthes, 1989). A low-level divergence and convergence below 2000 m form downdraft and updraft extending upward with the maximum amplitude at 2000 m, respectively (Fig. 12b). Divergence and convergence also appears alternately in the vertical direction. These divergence patterns are consistent with the vertical

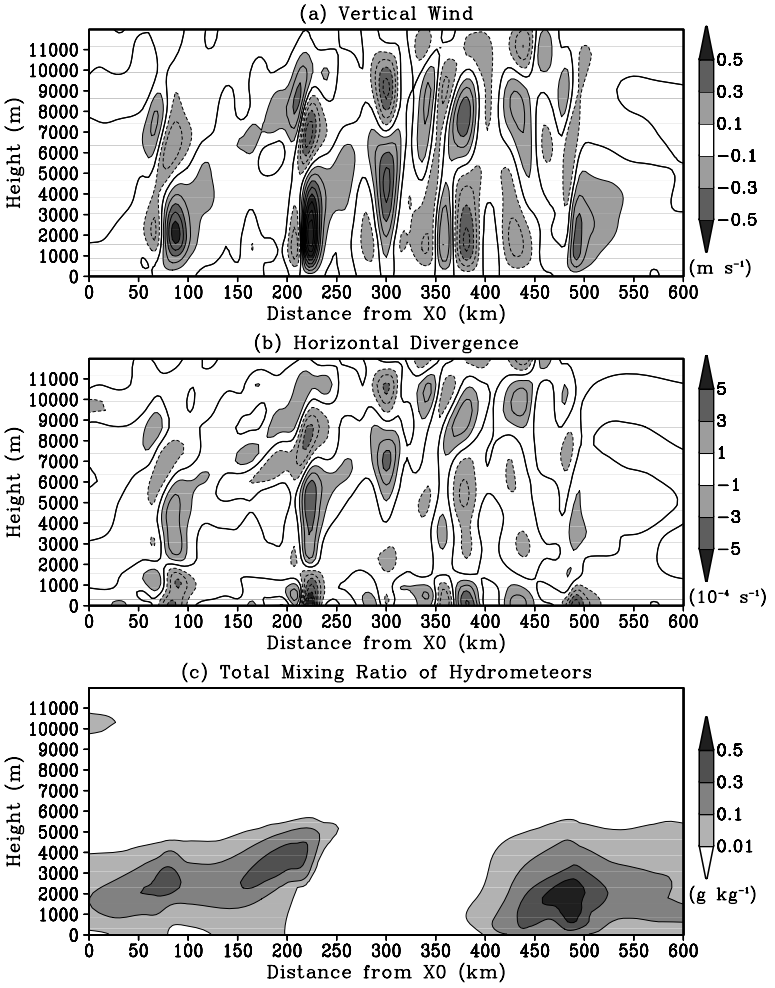

Fig. 12. Vertical cross sections of (a) vertical velocity (m s^{-1}), (b) horizontal divergence (10^{-4} s^{-1}) and (c) total mixing ratio of hydrometeors (g kg^{-1}) along the line X0-X1 in Fig. 11 at 0000 UTC, 22 December 2000 obtained from the numerical experiment. The contour intervals are (a) 0.1 m s^{-1} and (b) 1×10^{-4} s^{-1}, respectively.

velocity patterns in the point of the mass continuity. Figure 12c shows the total mixing ratio of hydrometeors. The mixing ratio more than 0.01 g kg^{-1} is present below a height of about 5000 m for less than X = 250 km and more than 380 km. Some peaks correspond to the maximum updrafts. On the other hand, in the region between X = 250 and 380 km, the hydrometeor mixing ratio is negligible and does not correspond to each updraft. In this region, there is mesoscale descending motion coinciding with the reverse tip jet and relative humidity is approximately 60–90% (not shown). This relative humidity appears insufficient for a generation of hydrometeors.

The relationship of this wave-like pattern and the location of topography is shown in Fig. 13. As shown in Fig. 1, there are fiords along the coastal area of Greenland. The vertical velocity (Fig. 13a) shows rising motion downstream of the valleys and sinking motion on the lee sides of the hills. The vertical velocity is in phase at least to a height of 3071 m. The horizontal divergence field (Fig. 13b) shows a convergence in the downward side of the valley and a divergence behind the hill in the low level. This pattern becomes unclear at a height of 1549 m and then at a height of 3071 m shows the opposite pattern with the low level. The horizontal wind speed (Fig. 13c) also shows a wave-like pattern. The wind speed at a height of 50 m is the largest along the coastal region, decreases downwind, and changes about 5 m s^{-1} in the normal direction to the wave crest. The strong wind lines appears to be located in the leeward side of hill tops in fiords. These locations are almost same as those of downward motions. Although the wind turns clockwise upward, less clear wave-like pattern of wind speed is still seen along the coastal region in the upper level.

Figure 14a shows the total surface heat flux, which is a sum of latent and sensible heat fluxes. In the present study, only the fluxes over the sea are discussed. The maximum total heat flux, more than 300 W m^{-2}, is co-located with the reverse tip jet (Fig. 6c). The region with total heat flux more than 100 W m^{-1} extends westward along the surface streamlines from the maximum total flux. There is also a region with large total heat flux along the east coast of Greenland. The latent heat flux (Fig. 14b) shows large values toward the west from Cape Farewell and near the eastern coast of Greenland, which shows a similar pattern as

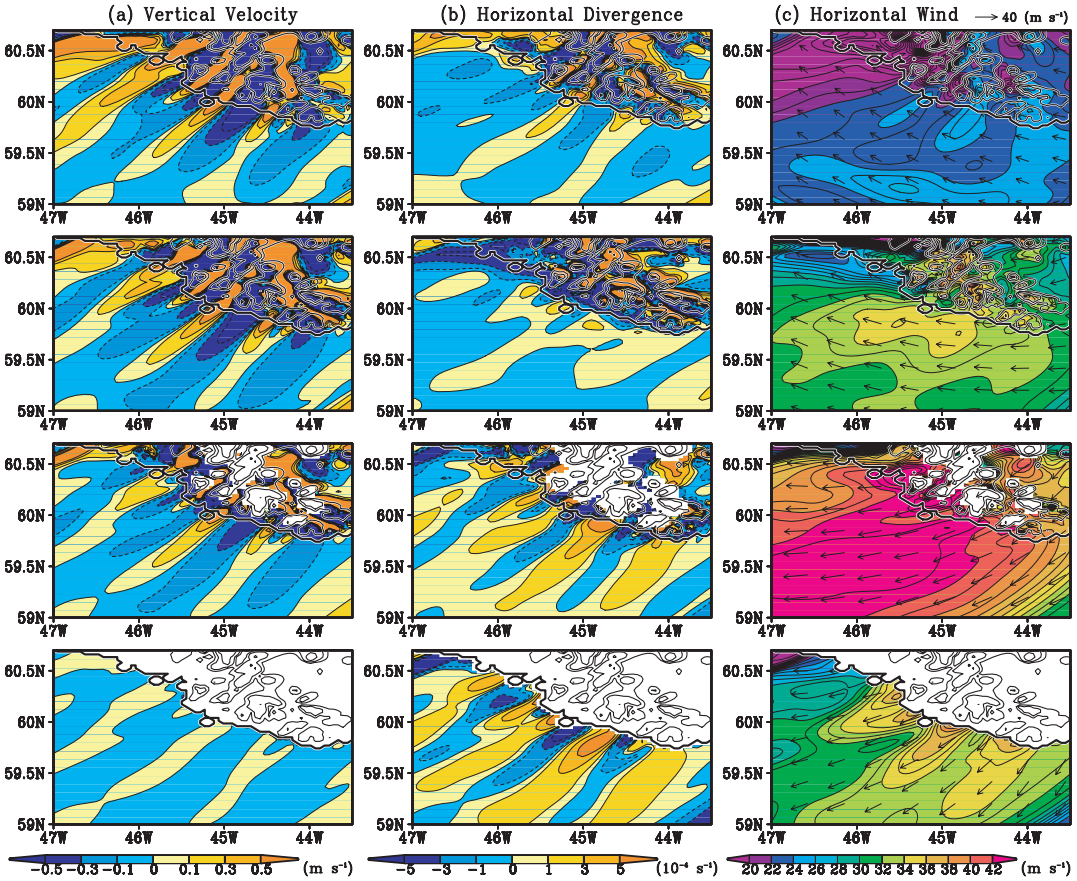

Fig. 13. Horizontal displays of (a) vertical velocity (m s^{-1}), (b) horizontal divergence (10^{-4} s^{-1}) and (c) horizontal velocity vectors (arrows) and wind speed (colour scales) at 0000 UTC, 22 December 2000 obtained from the numerical experiment. The fields at heights of 3071, 1549, 860 and 50 m are shown from upper to lower panels. The contour interval of wind speed in (c) is 1 m s^{-1}. Altitude of topography is also shown at 200, 500 and 1000 m by thick solid lines in all the panels.

that of total heat flux. The maximum latent heat flux is more than 150 W m^{-2}. The locations of maximum latent heat flux are scattered to the west of Cape Farewell. In addition, the moderate latent heat flux extends northward in the west of Greenland. The sensible heat flux (Fig. 14c) is also large in the strong wind region of the reverse tip jet. The maximum value of the sensible heat flux is more than 150 W m^{-2}, which is comparable with that of the latent heat flux. The positive sensible heat flux region does not extend northward as compared with the latent heat flux. The sharp edge shown in the total surface heat flux near the east coast (Fig. 14a) is seen in both of the latent and sensible heat fluxes (Figs. 14b and c).

In order to examine the pattern seen in the latent heat flux field, the surface wind speed and the difference between the saturation specific humidity at the SST (q_s) and the specific humidity of surface air (q_a) are shown in Figs. 15a and b, respectively. According to bulk theory, the latent heat flux is proportional to both of the surface wind speed and $q_s - q_a$ (e.g. Gill, 1982). The large latent heat flux region corresponds to large surface wind speed and moderate value of $q_s - q_a$. This air with moderate $q_s - q_a$ extends southward from the northerly wind region along the east coast of Greenland. The contours of surface wind speed (Fig. 15a) show a serrated pattern in just the west of Cape Farewell. However this pattern is not present in $q_s - q_a$ (Fig. 15b). Therefore, the pattern of surface wind is responsible for the fine structure in the maximum value of the latent heat flux. It is interesting to note that in the wake region to the northwest of the reverse tip jet, there is a maximum in $q_s - q_a$ suggesting that the wake is a region with very dry air. For the sharp edge of the latent heat flux along the east coast, large gradients of both the surface wind speed and $q_s - q_a$ correspond to the edge and are important for the formation of the sharp edge.

On the other hand, the sensible heat flux is proportional to the surface wind speed (Fig. 15a) and the difference between the SST (Fig. 1) and the surface air temperature (Fig. 16). A large sensible heat flux associated with the reverse tip jet corresponds to a large surface wind speed (Fig. 15a). In the vicinity of Cape Farewell, a low air temperature extends westward within the northerly wind extending from the Greenland east coastal region (Fig. 16). This southward extension of cold air also contributes

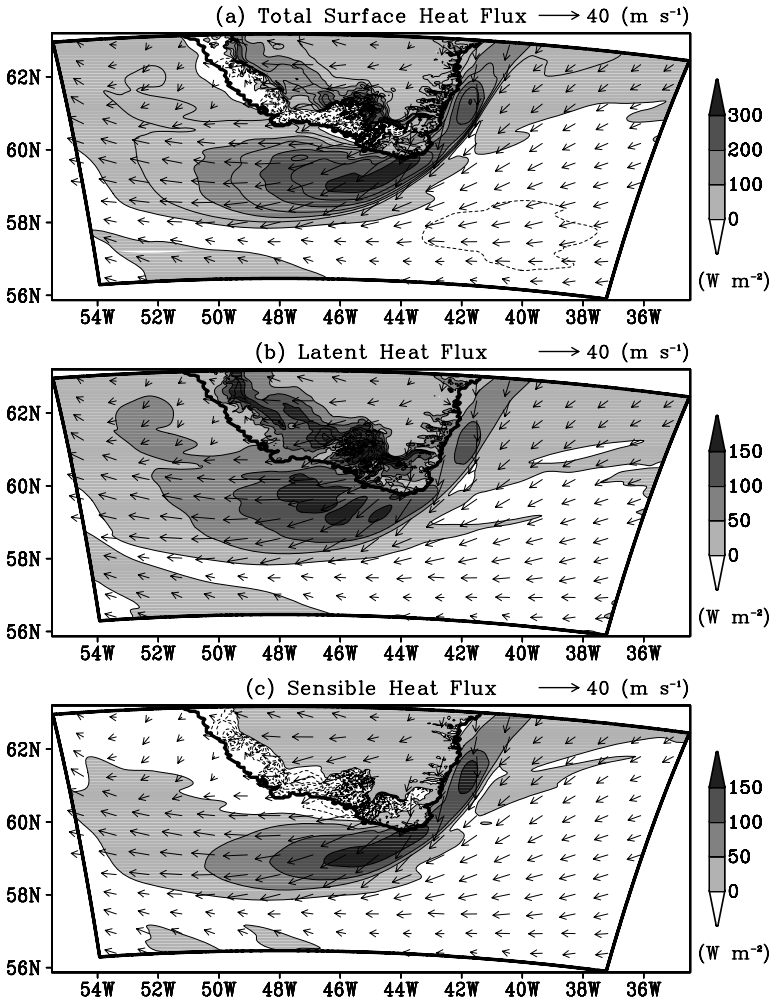

Fig. 14. Surface heat fluxes (contours and grey levels, W m^{-2}) and surface wind vectors (arrows) at 0000 UTC, 22 December 2000 obtained from the numerical experiment. (a) Total heat flux, (b) latent heat flux and (c) sensible heat flux. The contour interval is 50 W m^{-2}.

to the large sensible heat flux along the east coast of Greenland and just in the south of Cape Farewell. The eastern edge of the low air temperature field shows a sharp gradient. This large gradient in temperature coincides with the large surface wind speed (Fig. 15a) and moisture gradients (Fig. 15b), and they all are associated with the band cloud formed along the eastern edge of the reverse tip jet (Figs. 4, 9 and 10). The very dry region in the wake region in the west of Greenland (Fig. 15b) corresponds to a warm air at surface. This warm air decreases the temperature difference between the sea and air. This suppresses the sensible heat flux in the wake (Fig. 14c).

5. Discussion

In our simulation, the wind direction was northerly along the east coast of Greenland in the low level (Figs. 6 and 15a). This is consistent with composite analyses using the NCEP reanalysis data (Moore, 2003) and the Quik-SCAT satellite data (Moore and Renfrew, 2005). Moore (2003) and Moore and Renfrew (2005) suggested that reverse tip jets are related to barrier winds along the east coast of Greenland because this northerly wind near the east coast is clearly different from the upstream easterly flow. In addition, this northerly flow was confined below the inland topography of Greenland in the present study. For $N = 0.012$ s^{-1} and $U = 15$ m s^{-1} in the upstream low-level flow (62°N, 38°W), and $h = 2000$ m for the topography of southern Greenland (Fig. 1a) for the present case, $\hat{h}$ is 1.6, which indicates the flow toward Greenland is easily blocked. In the following discussion, we consider a parcel moving on a constant level without vertical motion and that the ambient pressure gradient is constant and is directed to the south, where the ambient field means a field undisturbed by the Greenland topography. No turbulent mixing is also taken into consideration. A conceptual model showing acceleration processes of a parcel in the reverse tip jet is shown in Fig. 17. From the simulation results (Fig. 8), the flow is geostrophic far upstream of Cape Farewell. As the parcel moves toward Greenland, it is blocked and decelerates. At this point (point I in Fig. 17), the flow is subgeostrophic and the pressure gradient force ($|\mathbf{F}_p|$) exerted on the parcel is greater than the Coriolis force ($|\mathbf{F}_c|$). This results in a turning of

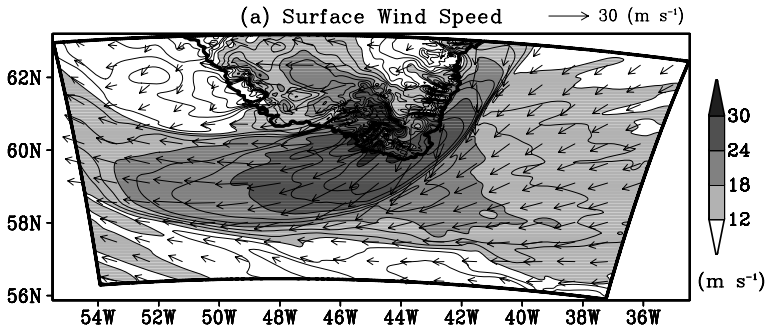

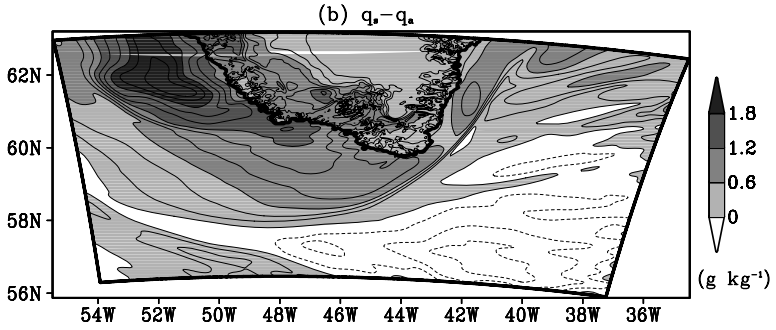

Fig. 15. (a) Surface velocity vectors (arrows) and wind speed (contours and grey levels, m s^{-1}) and (b) difference between saturation specific humidity at ground and sea surface temperature and specific humidity in the surface air (g kg^{-1}) at 0000 UTC, 22 December 2000 obtained from the numerical experiment. The contour intervals are (a) 2 m s^{-1} and (b) 0.2 g kg^{-1}, respectively.

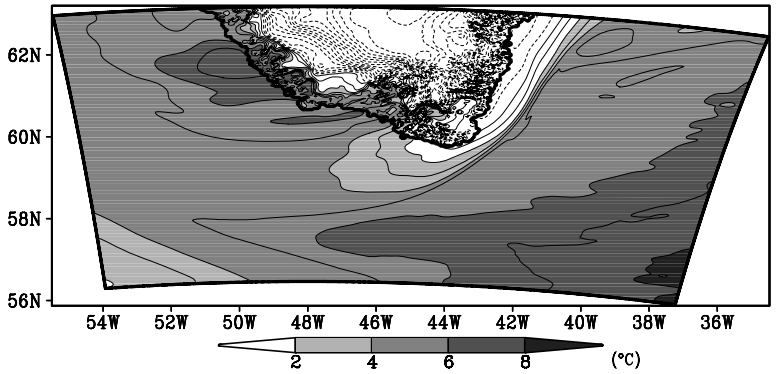

Fig. 16. Surface air temperature (°C) at 0000 UTC, 22 December 2000 obtained from the numerical experiment. The contour interval is 1 °C.

the parcel toward the low pressure side, that is the left-side of the geostrophic flow, and the parcel moves toward the south (the northerly flow) along the east coast of Greenland (Fig. 5c). As the parcel moves toward the $\mathbf{F}_p$ vector, it is accelerated and becomes supergeostrophic (point II in Fig. 17). When the parcel continues to be accelerated, $\mathbf{F}_c$ causes a turning of the parcel to the right-hand side. This indicates an anticyclonic turning (Figs. 6c and 15a), as pointed out for the reverse tip jet in Moore and Renfrew (2005). The parcel is finally directed to the high pressure side and is decelerated by $\mathbf{F}_p$ (point III in Fig. 17). Godske et al. (1957) pointed out that a flow toward an obstacle shows a strong wind at the left corner of the obstacle in the northern hemisphere. They referred to this effect of an obstacle causing a strong wind as the 'corner effect'. On the other hand, Barstad and Grønås (2005, 2006) referred to similar strong winds over southern Norway as the 'left-side jet'. The eastern part of the reverse tip jet appears to be a same type of strong wind as the jet by the corner effect and left-side jet. Some literatures have also mentioned the upstream turning of flows down the large-scale pressure gradient (the left-side deflection in the northern hemisphere) in crossing mountain ranges and the increase in the wind speed of the flows (e.g. Smith, 1982; Skeie and Grønås, 2000).

In the northwest part of the reverse tip jet, motion in the low level cannot be restricted at a constant level because of the presence of the topography (Fig. 6c). The quantitative contribution to the jet formation by the vertical motion should be carefully estimated in future work.

The deflected northerly wind along the east coast of Greenland makes a convergence with the ambient easterly flow. This dynamical orographic effect appears to be the primary role to make the convergence line. In addition, the deflected northerly flow causes cold advection from Greenland toward the sea (not shown) to make the sharp temperature gradient near the surface along the convergence line (Fig. 16). These results in the long moderate updraft (Fig. 11) and relatively tall banded cloud (Figs. 9 and 10) along the east coast of Greenland and the

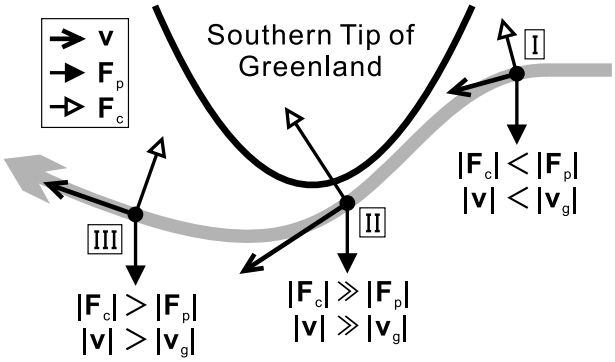

Fig. 17. Conceptual model showing acceleration processes of a parcel in the reverse tip jet. A thick grey line with an arrow indicates the trajectory of the parcel. Thin, solid, and white arrows represent the wind (**v**), pressure gradient force ($\mathbf{F}_p$), and Coriolis force ($\mathbf{F}_c$) vectors, respectively. The geostrophic wind is designated by $\mathbf{v}_g$. At the points I, II and III, the flows is subgeostrophic, highly supergeostrophic and moderately supergeostrophic, respectively.

eastern edge of the reverse tip jet. This band was also confirmed in satellite images during this reverse tip jet event (Fig. 4a). This narrow banded cloud coincides with sharp gradients of wind speed (Fig. 15a), temperature (Fig. 16), and moisture (Fig. 15b) of surface air. These cause a sharp contrast of surface heat flux across the banded cloud (Fig. 14).

A wave-like change of horizontal wind speed shown in Figs. 11–13 appears to correspond to the topography of the fiords along the coastal region of Greenland, namely, local maxima of horizontal wind speed was present in the lee side of hill tops associated with fiord topography. We consider this flow associated with fiords as that over a mountain ridge with a gap. Saito (1993) showed a regime diagram of flows over a mountain ridge with a gap as a function of the non-dimensional mountain height. From his simulation result, upstream wind speed on the surface is accelerated in the lee of both the gap and the peak. However, the locations of the wind speed maxima on the surface are different among the regimes. For the low mountain case ($\hat{h} \ll 1$), the maximum wind speed is present in the lee side of the peak, which corresponds to downslope winds. On the other hand, for the very high mountain case ($\hat{h} > \sim 2$), strong winds are seen in the lee of the gap and weak winds behind the peak. This high winds formed in the lee of gap correspond to gap winds. In the middle height case, wind speed maximum associated with hydraulic jump is present just behind the peak, and then, in farther downstream, wind speed maximum is seen in the lee of gap. Pan and Smith (1999) also performed similar simulations and their results are consistent with Saito (1993). In the vicinity of Cape Farewell, topography associated with fiords is isolated from large topography located in the centre of Greenland and flat and low-altitude ground extends in the upstream (northeast) of fiords. For this fiords, the low-level (less than about a height of 1100 m) atmospheric stratification N in the upstream part (60.4°N, 43.7°W) is 0.015 s^{-1}, the upstream surface velocity is more than 20 m s^{-1}, and a height of peak is less than 1000 m. Then, the non-dimensional mountain height is less than 0.75, in which a wind speed maximum appears in the lee of the peak according to Saito's regime diagram. This is consistent with the flow around fiords in the present case. Therefore, the wave-like pattern can be related to downslope winds behind mountains with fiords.

Although the wave-like pattern was located within the reverse tip jet in the present case, this is also seen in the wake to the north of the reverse tip jet. This indicates that the momentum transports associated with the wave-like vertical winds do not explain a whole formation of the reverse tip jet. However, this fine wave-like wind speed maxima can cause much stronger winds to local areas superimposing on the strong wind region associated with more wider Greenland topography (Fig. 13c).

6. Summary

A reverse tip jet was formed from 21 to 22 December 2000 in the vicinity of Cape Farewell, which is located at the southern tip of Greenland. The fine structures of the reverse tip jet are studied using a numerical model, Cloud Resolving Storm Simulator (CReSS), with a horizontal resolution of 3 km to understand the non-composite feature of reverse tip jets.

When a synoptic-scale cyclone propagated toward Iceland over the North Atlantic, high and low pressure region were formed at the north and the south around Cape Farewell, respectively. This resulted in easterly surrounding wind around southern Greenland. Farther upstream of Greenland at a height of 500 m, the wind speed was comparable with the geostrophic wind speed which was 15 m s^{-1}. In this situation, a reverse tip jet formed from the southeastern coast of Greenland to the west of Cape Farewell. The maximum wind speed in excess of 45 m s^{-1} was present at a height of 500 m near the coast to the west of Cape Farewell. Along the upwind coastal region, the wind direction below a height of 2000 m was northerly and was directed from the high pressure side to the low pressure side. The wind speed in the reverse tip jet region was significantly larger than that of the upstream flow and was highly supergeostrophic. This flow anticyclonically turned along its streamline and was finally directed toward the high pressure side against the pressure gradient force. This anticyclonic turning is consistent with a composite feature shown in Moore and Renfrew (2005).

Along the east coast of Greenland and eastern edge of the reverse tip jet, a banded cloud was formed. This band was located between the northerly flow deflected by Greenland and the upstream easterly flow. The location of the band also coincided with a large gradient of temperature between cold air along the coast and the warmer upstream air in the low level. The cold air was caused by cold advection with the Greenland-deflected northerly flow. This temperature contrast could somewhat

contribute to the formation of the band. The large gradients of wind speed, temperature, and moisture along the band cloud resulted in a sharp gradient of surface heat flux. Within the reverse tip jet, a cloud free region was present. This feature would indicate that a mesoscale descending motion was present in this region. This cloud free region also corresponds to the anticyclonic flow part. To the north of the cloud free region coincident with the reverse tip jet, hydrometeors were significant again. The hydrometeors in this region were formed by wave-like updrafts. The wave-like vertical velocity pattern appears to be related to downslope winds behind the mountain peaks with fiord topography present in coastal Greenland and propagate vertically as gravity waves. This updraft pattern was consistent with the low-level divergence below a height of 1500 or 2000 m. Although the wave-like updrafts were seen along the southwest of southern Greenland, no hydrometeors were formed in not so high relative humidity within the reverse tip jet. The wave-like pattern seen in the lee side of Greenland made a fine distribution of surface heat flux.

The total heat flux more than 300 W m^{-2} from the sea surface coincided with the reverse tip jet. Both maxima of latent and sensible heat fluxes were 150 W m^{-1} and were located at almost the same region as the maximum of total heat flux. This large surface heat flux to the southwest of Cape Farewell is located in the vicinity of a deep mixed layer region of ocean shown in Lavender et al. (2002). To the northwest of the reverse tip jet, very dry and warm air was present. The dry and warm air in this region could imply a descending flow in a wake behind the high Greenland topography. The very dry air allows for moderate latent heat fluxes. On the contrary, higher surface air temperature suppresses sensible heat flux. Therefore, the total heat flux is not large in the wake.

As mentioned in Moore (2003) and Moore and Renfrew (2005), barrier winds can be responsible for the strong wind of the reverse tip jet along the eastern coast of Greenland because the upstream non-dimensional mountain height $\hat{h}$ was more than 1 and, as a result, the flow was easily deflected by the Greenland topography. The wind speed of the blocked flow once decreases. This appears to correspond to the subgeostrophic flow along the east coast of Greenland. Then, this subgeostrophic flow is turned toward the low pressure side with the decreased Coriolis force and is accelerated by the pressure gradient force. This would finally cause the highly supergeostrophic flow with anticyclonic curvature which was seen in the core of the reverse tip jet. In the above-mentioned mechanism, a vertical motion is not necessarily present. However, in the northwest part of the reverse tip jet, the flow needs to move vertically because of the presence of the Greenland topography. This quantitative contribution of the vertical motion to the formation of the reverse tip jet remains to be studied. The wave-like pattern, which would be related to fiords along the coast, in the lee side of Greenland locally caused the fine wind maxima superimposing on the whole reverse tip jet region.

The routine observations are insufficient to validate whole structures obtained by simulations. It is expected that the aircraft-based field campaign, which was performed around Greenland (Renfrew et al., 2008), provides a lot of observational evidence.

7. Acknowledgments

The authors would like to thank Ms. Rebekah Martin, the University of Toronto, for performing the simulation using MM5. We also thank Mr. Hendra Adiwidjaja, the University of Toronto, for preparing the observational data. Thanks are extended to reviewers for their comments which greatly contributed to improve the manuscript. The CReSS simulation was performed at bluevista of Computational and Information Systems Laboratory of the National Center for Atmospheric Research (NCAR). GrADS was used for drawing the figures. Support for this research was provided by the Canadian Foundation for Climate and Atmospheric Sciences.

References

Asselin, R. 1972. Frequency filter for time integrations. *Mon. Wea. Rev.* **100**, 487–490.

Baines, P. G. 1987. Upstream blocking and airflow over mountains. *Ann. Rev. Fluid Mech.* **19**, 75–97.

Barstad, I. and Grønås, S. 2005. Southwesterly flows over southern Norway–Mososcale sensitivity to large-scale direction and speed. *Tellus* **57A**, 136–152.

Barstad, I. and Grønås, S. 2006. Dynamical structures for southwesterly airflow over southern Norway: the role of dissipation. *Tellus* **58A**, 2–18.

van den Broeke, M. R. and Gallee, H. 1990. Observation and simulation of barrier winds at the western margin of the Greenland ice sheet. *Quart. J. Roy. Meteor. Soc.* **122**, 1365–1383.

Chen, W.-D. and Smith, R. B. 1987. Blocking and deflection of airflow by the Alps. *Mon. Wea. Rev.* **115**, 2578–2597.

Cotton, W. R. and Anthes, R. A. 1989. *Storm and Cloud Dynamics*. Academic Press, San Diego, CA, 883 pp.

Doyle, J. D. and Shapiro, M. A. 1999. Flow response to large-scale topography: The Greenland tip jet. *Tellus* **51A**, 728–748.

Endo, S., Shinoda, T., Tanaka, H., Hiyama, T., Tsuboki, K., and co-authors. 2008. Characteristics of vertical circulation in the convective boundary layer over the Huaihe River Basin in China in the early summer of 2004. *J. Appl. Meteor. Climatol.* **47**, 2911–2928.

Flamant, C., Drobinski, P., Nance, L., Banta, R., Darby, L. and co-authors. 2002. Gap flow in an Alpine valley during a shallow south föhn event: observations, numerical simulations and hydraulic analogue. *Quart. J. Roy. Meteor. Soc.* **128**, 1173–1210.

Gaberšek, S. and Durran, D. R. 2004. Gap flows through idealized topography. Part I: forcing by large-scale winds in the nonrotating limit. *J. Atmos. Sci.* **61**, 2846–2862.

Gaberšek, S. and Durran, D. R. 2006. Gap flows through idealized topography. Part II: effects of rotation and surface friction. *J. Atmos. Sci.* **63**, 2720–2739.

Gill, A. E. 1982. *Atmosphere-Ocean Dynamics*. Academic Press, San Diego, CA, 662 pp.

Godske, C. L., Bergeron, T., Bjerknes, J. and Bundgaard, R. C. 1957. *Dynamic Meteorology and Weather Forecasting*. American Meteorological Society, Boston, MA and Carnegie Institution of Washington, Washington, DC., 800 pp.

Grell, G. A., Dudhia, J. and Stauffer, D. R. 1995. *NCAR Technical Note "A Description of the Fifth-Generation Penn State/NCAR Mesoscale Model (MM5)"*. NCAR, Boulder, CO, 122 pp.

Jackson, P. L. and Steyn, D. G. 1994a. Gap winds in a fjord. Part I: Observations and numerical simulation. *Mon. Wea. Rev.* **122**, 2645–2665.

Jackson, P. L. and Steyn, D. G. 1994b. Gap winds in a fjord. Part II: hydraulic analog. *Mon. Wea. Rev.* **122**, 2666–2676.

Klemp, J. B. and Wilhelmson, R. B. 1978. The simulation of three-dimensional convective storm dynamics. *J. Atmos. Sci.* **35**, 1070–1096.

Lavender, K. L., Davis, R. E. and Owens, W. B. 2002. Observations of open-ocean deep convection in the Labrador Sea from subsurface floats. *J. Phys. Oceanogr.* **32**, 511–526.

Lilly, D. K. 1978. A severe downslope windstorm and aircraft turbulence event induced by a mountain wave. *J. Atmos. Sci.* **35**, 59–77.

Liu, A. Q., Moore, G. W. K., Tsuboki, K. and Renfrew, I. A. 2004. A high-resolution simulation of convective roll clouds during a cold-air outbreak. *Geophys. Res. Lett.* **31**, L03101, doi:10.1029/2003GL018530.

Liu, A. Q., Moore, G. W. K., Tsuboki, K. and Renfrew, I. A. 2006. The effect of the sea-ice zone on the development of boundary-layer roll clouds during cold air outbreaks. *Bound.-Layer Meteor.* **118**, 557–581.

Maesaka, T., Moore, G. W. K., Liu, Q. and Tsuboki, K. 2006. A simulation of a lake effect snowstorm with a cloud resolving numerical model. *Geophys. Res. Lett.* **33**, L20813, doi:10.1029/2006GL026638.

Martin, R. and Moore, G. W. K. 2007. Air-sea interaction associated with a Greenland reverse tip jet. *Geophys. Res. Lett.* **34**, L24802, doi:10.1029/2007GL031093.

Moore, G. W. K. 2003. Gale force winds over the Irminger Sea to the east of Cape Farewell, Greenland. *Geophys. Res. Lett.* **30**, 1894, doi:10.1029/2003GL018012.

Moore, G. W. K. and Renfrew, I. A. 2005. Tip jets and barrier winds: a QuikSCAT climatology of high wind speed events around Greenland. *J. Climate* **18**, 3713–3725 (corrigendum is provided at 4919).

Moore, G. W. K., Pickart, R. S. and Renfrew, I. A. 2008. Buoy observations from the windiest location in the world ocean, Cape Farewell, Greenland. *Geophys. Res. Lett.* **35**, L18802, doi:10.1029/2008GL034845.

O'Connor, W. P., Bromwich, D. H. and Carrasco, J. F. 1994. Cyclonically forced barrier winds along the Transantarctic Mountains near Ross Island. *Mon. Wea. Rev.* **122**, 137–150.

Ohigashi, T. and Tsuboki, K. 2007. Shift and intensification processes of the Japan-Sea Polar-Airmass Convergence Zone associated with the passage of a mid-tropospheric cold core. *J. Meteor. Soc. Japan* **85**, 633–662.

Pan, F. and Smith, R. B. 1999. Gap winds and wakes: SAR observations and numerical simulations. *J. Atmos. Sci.* **56**, 905–923.

Parish, T. R. 1982. Barrier winds along the Sierra Nevada Mountains. *J. Appl. Meteor.* **21**, 925–930.

Pickart, R. S., Spall, M. A., Ribergaard, M. H., Moore, G. W. K. and Milliff, R. F. 2003. Deep convection in the Irminger Sea forced by the Greenland tip jet. *Nature* **424**, 152–156.

Renfrew, I. A., Moore, G. W. K., Kristjánsson, J. E., Ólafsson, H., Gray, S. L. and co-authors. 2008. The Greenland Flow Distortion experiment. *Bull. Amer. Meteor. Soc.* **89**, 1307–1324.

Saito, K. 1993. A numerical study of the local downslope wind "Yamaji-kaze" in Japan. Part 2: non-linear aspect of the 3-D flow over a mountain range with a col. *J. Meteor. Soc. Japan* **71**, 247–271.

Saito, K. and Ikawa, M. 1991. A numerical study of the local downslope wind "Yamaji-kaze" in Japan. *J. Meteor. Soc. Japan* **69**, 31–56.

Serreze, M. C., Carse, F., Barry, R. G. and Rogers, J. C. 1997. Icelandic low cyclone activity: climatological features, linkages with the NAO, and relationships with recent changes in the northern hemisphere circulation. *J. Climate* **10**, 453–464.

Sharp, J. and Mass, C. 2002. Columbia Gorge gap flow. *Bull. Amer. Meteor. Soc.* **83**, 1757–1762.

Skeie, P. and Grønås, S. 2000. Strongly stratified easterly flows across Spitsbergen. *Tellus* **52A**, 473–486.

Smith, R. B. 1982. Synoptic observations and theory of orographically wind and pressure. *J. Atmos. Sci.* **39**, 60–70.

Steenburgh, W. J., Schultz, D. M. and Colle, B. A. 1998. The structure and evolution of gap outflow over the Gulf of Tehuantepec, Mexico. *Mon. Wea. Rev.* **126**, 2673–2691.

Tsuboki, K. and Sakakibara, A. 2002. Large-scale parallel computing of cloud resolving storm simulator. *High Performance Computing* (eds. H. Zima et al). Springer-Verlag, Berlin-Heidelberg, 243–259.

Tsuboki, K. and Sakakibara, A. 2007. *Numerical Prediction of High-Impact Weather Systems –The Textbook for Seventeenth IHP Training Course in 2007–*. Hydrospheric Atmospheric Research Center, Nagoya, Japan, 281 pp.

Wang, C.-C., Chen, G. T.-J., Chen, T.-C. and Tsuboki, K. 2005. A numerical study on the effects of Taiwan topography on a convective line during the mei-yu season. *Mon. Wea. Rev.* **133**, 3217–3242.

Yamada, H. 2008. Numerical simulations of the role of land surface conditions in the evolution and structure of summertime thunderstorms over a flat highland. *Mon. Wea. Rev.* **136**, 173–188.

Yamada, H., Geng, B., Uyeda, H. and Tsuboki, K. 2007a. Role of the heated landmass on the evolution and duration of a heavy rain episode over a Meiyu-Baiu frontal zone. *J. Meteor. Soc. Japan* **85**, 687–709.

Yamada, H., Geng, B., Uyeda, H. and Tsuboki, K. 2007b. Thermodynamic impact of the heated landmass on the nocturnal evolution of a cloud cluster over a Meiyu-Baiu front. *J. Meteor. Soc. Japan* **85**, 663–685.

Zhang, C.-Z., Uyeda, H., Yamada, H. and Geng, B. 2006. Characteristics of convections of medium depth to south of the meiyu front analyzed by using numerical simulation. *Sci. Online Lett. Atmos.* **2**, 160–163.